Pramana – J. Phys., Vol. 39, No. 5, November 1992, pp. 509–520. © Printed in India.

Routes to chaos and mode-locking in interferometers with nematic film inserts

S RAJASEKAR

Material Science Division, Indira Gandhi Centre for Atomic Research, Kalpakkam 603 102, India

MS received 15 July 1992; revised 7 September 1992

Abstract. The influence of time-dependent periodic optical drive in the Fabry-Perot interferometer system has been investigated using a theoretical model equation. A variety of features such as different routes to chaos, multiperiodic oscillations, coexistence of multiple attractors and mode-locking with devil's staircase are found to occur for a certain range of parametric values.

Keywords. Fabry-Perot interferometer; routes to chaos; multiperiodic oscillations; mode-locking.

PACS Nos 05·45; 42·50; 42·65; 47·20

1. Introduction

In recent years a great deal of interest has been devoted to exploring the complexity of nonlinear dynamical systems. Periodic and chaotic motions have been found to occur in nonlinear optical devices (Cheung *et al* 1983; Dangoisse *et al* 1990; Sasa 1990). Nematic liquid crystals are a kind of highly nonlinear optical medium. They have strong optical nonlinearity arising from the optical-field-induced collective reorientation of molecules (Durbin *et al* 1981a; Csillag *et al* 1981; Herman and Serinko 1979). The dynamical behavior of an interferometer system with a nematic film inside and irradiated with a cw laser beam has been studied both experimentally and theoretically. In this system the liquid crystal molecules play the role of a driven nonlinear oscillator. Many nonlinear optical effects such as nonlinear diffraction (Khoo and Zhuang 1982), wave mixing (Durbin *et al* 1981b, 1982), instabilities (Cheung *et al* 1983; Zuniga 1990) were observed.

Recently the influence of time-dependent periodic optical drive in the Fabry-Perot interferometer system has been carried out both experimentally and numerically solving the theoretical model equation (Wang *et al* 1990). The system was found to exhibit transition to chaos through period doubling bifurcation and quasiperiodicity by numerical analysis. Experimentally quasiperiodic oscillation was found. A good agreement between the experimental observation and numerical analysis was obtained. However, a detailed study of dynamical behavior of theoretical model equation is still not available in the literature. The prime aim of the present paper is to investigate the possible routes to chaos, mode-locking behavior and characterization of regular and chaotic motions in the Fabry–Perot interferometer (FPI) system.

The paper is organized as follows. The mathematical model for the FPI system is

described in § 2. Various routes to chaos and mode-locking behavior are studied in § 3. Also we show the occurrence of mixed mode oscillations for specific parametric choices. Finally, § 4 contains summary and conclusion.

2. Description of FPI model

We consider an FPI system with a nematic liquid crystal sandwiched between two dielectric mirrors. A linearly polarized input beam from a laser nearly normally incident on the liquid crystal cell. A magnetic field is applied parallel to the laser polarization to induce an initial orientation of the nematic director. The periodic optical drive can be supplied by the external intensity-modulation function of laser. Let x and y represent the round-trip phase shifts induced by the laser-induced molecular reorientation and laser heating respectively. Then the dynamical equations for x and y can be written as (Cheung *et al* 1983; Wang *et al* 1990)

$$x' = \frac{1}{\tau_1}\left[-x + \frac{\alpha_1 K T_0 I_{in}(1 + f \sin \omega t)}{1 + F \sin^2\{(P + x + y)/2\}} \right], \tag{1a}$$

$$y' = \frac{1}{\tau_2}\left[-y + \frac{\alpha_2 K T_0 I_{in}(1 + f \sin \omega t)}{1 + F \sin^2\{(P + x + y)/2\}} \right] \tag{1b}$$

where τ_1 and τ_2 are the relaxation times and α_1 and α_2 are constants governing the strength of the laser-induced molecular reorientation and laser heating respectively. K is a constant which is related to the dispersion of the FPI, T_0 is the peak transmission and F is the finesse of the interferometer, and P is the initial round-trip phase shift. $I_{in}(1 + f \sin \omega t)$ describes the periodic nature of the input intensity with I_{in} as the constant input part, f and ω are the drive amplitude and frequency respectively. Defining $z = \omega t$, $A = \alpha_1 K T_0 I_{in}$ and $B = \alpha_2 K T_0 I_{in}$, equation (1) becomes

$$x' = \frac{1}{\tau_1}\left[-x + \frac{A(1 + f \sin z)}{1 + F \sin^2\{(P + x + y)/2\}} \right], \tag{2a}$$

$$y' = \frac{1}{\tau_2}\left[-y + \frac{B(1 + f \sin z)}{1 + F \sin^2\{(P + x + y)/2\}} \right], \tag{2b}$$

$$z' = \omega. \tag{2c}$$

The experimental set up of the FPI system with a nematic liquid crystal film was discussed in detail by Wang *et al* (1990). Qualitative behavior of the FPI can be predicted from the numerical solution of (2). Even though bistability and chaotic dynamics in the above system have been observed experimentally (Cheung *et al* 1983; Wang *et al* 1990) and through numerical integration of (2) (Wang *et al* 1990), a detailed investigation of (2) concerning the bifurcations and mode-locking phenomena has not been studied. In this paper we therefore want to give examples of bifurcation diagrams of system (2) showing various bifurcation sequences. Further, we study the mode-locking regions using the generalized winding number (Parlitz and Lauterborn 1987).

3. Chaotic behavior

In this section various dynamical behavior of FPI system will be described in detail. For analysis we take $\tau_1 = 125$, $\tau_2 = 1$, $A = 6{\cdot}37$, $B = -0{\cdot}98$, $P = 4$ and $F = 30$, the values used by Cheung *et al* (1983) and Wang *et al* (1990). The initial values in the numerical calculations are fixed at $x(0) = 3$ and $y(0) = 0$. We study the behavior of the system (2) for various ranges of f and ω values. For $f = 0$, equation (2) is a 2-dimensional autonomous system and hence it does not show chaotic behavior. In the following we show the occurrence of various routes to chaos, multiperiodic oscillations and coexistence of multiple orbits under the influence of periodic drive.

3.1 *Intermittent chaos*

Figure 1a shows the bifurcation phenomenon where the values of x at every period of the external drive versus the driving amplitude f is plotted for $\omega = 0{\cdot}646$. Figure 1b shows the largest Lyapunov characteristic exponent (λ_m). For $f < 0{\cdot}159$ quasiperiodic

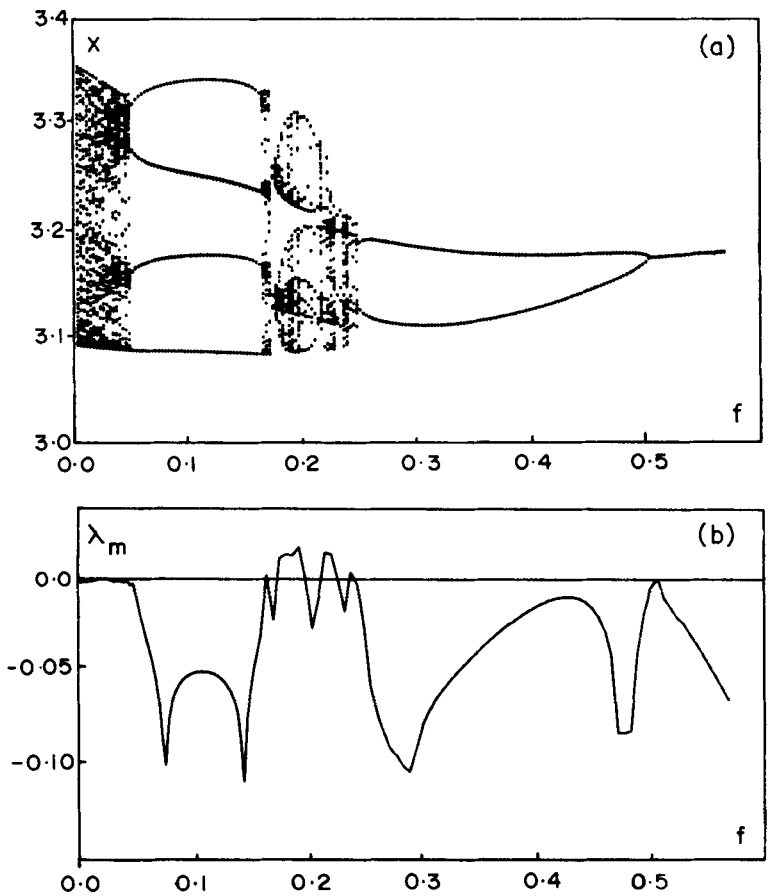

Figure 1. Bifurcation diagram (**a**) for $\omega = 0{\cdot}646$ showing the first coordinate x of the attractor in the Poincaré cross section versus the parameter f and the largest Lyapunov exponent (**b**).

and periodic oscillations with period-4 occurs. In this interval of f, λ_m is negative. Chaotic behavior interrupted by periodic windows is found to occur for $0{\cdot}159 < f < 0{\cdot}24$. In the chaotic regime λ_m is positive. When the driving amplitude is further increased periodic windows with higher periods exist and finally reverse bifurcation to period-1 attractor occurs.

Type I intermittent chaos are observed when the parameter f is increased from 0·159. To analyse the intermittency behavior we constructed a time series (x_n, y_n) defined by

$$x_n = x(t_0 + 2\pi n/\omega), \quad y_n = y(t_0 + 2\pi n/\omega), \quad n = 1, 2, \ldots, N$$

where $x(t)$, $y(t)$ are the solutions of (2). We then check the period, p, of the laminar parts and write the time series as if they were comprised of groups of length p. For example, we write the series $X = (x_n, y_n)$ as (Yasin *et al* 1991)

$$(X_1, \ldots, X_p, X_{p+1}, \ldots, X_{2p}, \ldots, X_{Lp+1}, \ldots, X_{(L+1)p}, \ldots, X_N),$$

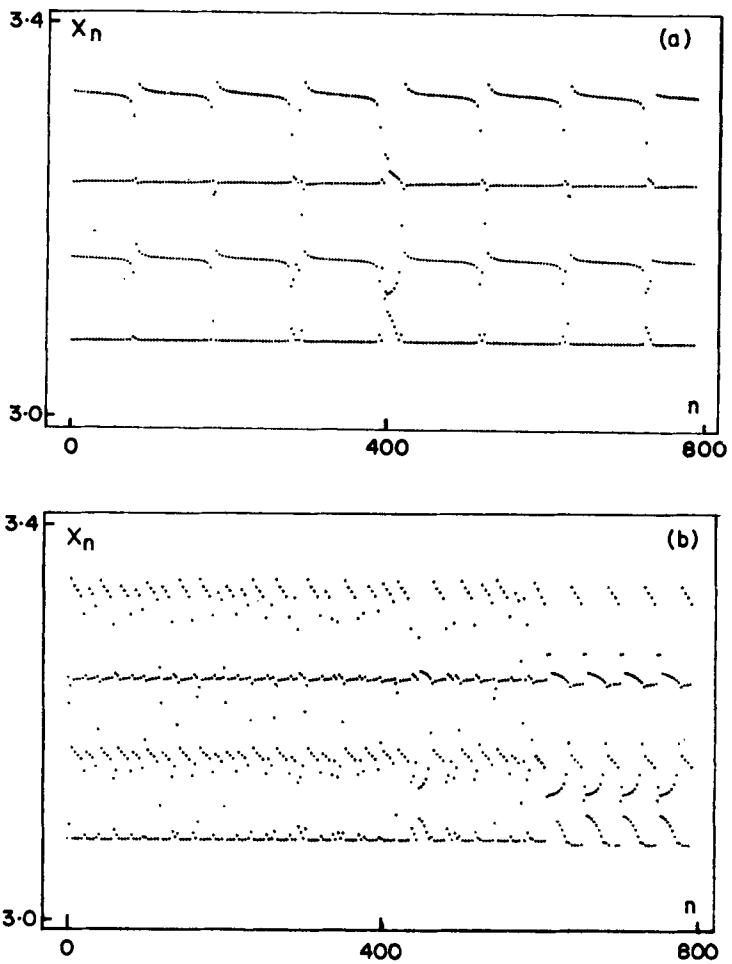

Figure 2. x_n vs n for (**a**) $f = 0{\cdot}159$ and (**b**) $f = 0{\cdot}161$ with $\omega = 0{\cdot}646$.

where $L < (N/p - 1)$. Next, a time series $\{X_n\}$ containing laminar parts alone is build up by removing the sudden bursting intervals such that X_j, X_{j+kp} (for arbitrary k) are closely valued numbers. As a demonstration, we show here figures for the cases $f = 0{\cdot}159$ and $0{\cdot}161$. The plot of x_n vs n in figure 2a for $f = 0{\cdot}159$ indicates that the laminar period is 4. When f is increased the laminar region decreases and the duration of chaotic bursts increase. The motion becomes fully chaotic for $f = 0{\cdot}161$ as shown in figure 2b. The plot of x_n vs x_{n+p} in figure 3 indicates that the intermittency to be of type I. Figure 4 shows the phase portrait of the chaotic motion for $f = 0{\cdot}161$ developed through the intermittent behavior.

Type I intermittent chaos is found to occur for various other parametric values also. In general, in the intermittent regime, we observed that if the transition to chaos occurs at $f \approx f_c$ as the parameter f is increased, then for $f < f_c (f > f_c)$ the motion is characterized by long(short) intervals of approximately periodic behavior interrupted by short (long) chaotic bursts occurring at irregular times.

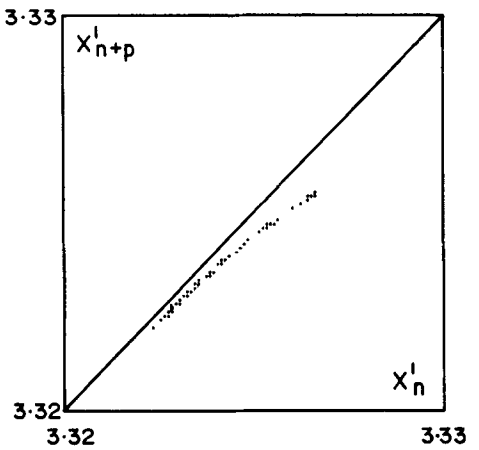

Figure 3. x_n vs x_{n+p} for $f = 0{\cdot}159$ and $\omega = 0{\cdot}646$.

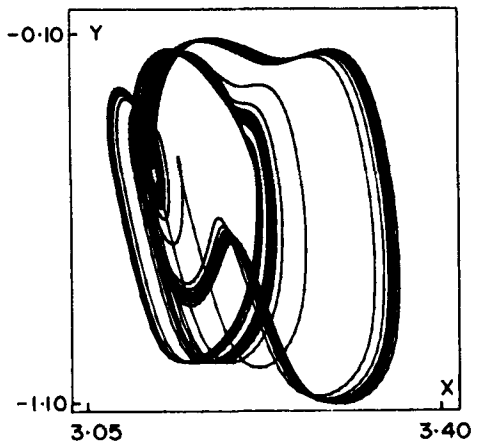

Figure 4. Chaotic attractor for $f = 0{\cdot}161$ and $\omega = 0{\cdot}646$.

3.2 *Multiperiodic oscillations*

We have studied the influence of ω on the behavior of the system (2) for a fixed value of f. Periodic and quasiperiodic oscillations, period doubling bifurcations and multiperiodic oscillations have been observed for $0 < \omega < 6$ with $f = 0{\cdot}2$. These features are illustrated in figure 5a, b, c. Various oscillating modes are not clearly visible in figure 5a. For clarity, a section of figure 5a showing the details of the interval $0{\cdot}3 < \omega < 1{\cdot}5$ is given in figure 5b. Between ω intervals we observed a series of mode-locked states with multiperiodic orbits $\pi(m)$ and mixed oscillation modes $\pi_{p,q}(m, m+1)$ consisting of p times of m-periodic orbits and q times of $m+1$-periodic orbits and chaotic orbits. This bifurcation diagram (5b) clearly illustrates the sequence of $\pi(m)$ modes with $m = 1, 2, \ldots, 8$. Between successive periods adding sequence chaotic motions and mixed modes of oscillation occur. Further, the regime of $\pi(m)$ modes decreases with increase in m value. Figure 5c shows the regime of the mixed modes between two neighbouring modes $\pi(2)$ and $\pi(3)$.

3.3 *Generalized winding numbers and devil's staircase*

Besides bifurcation diagrams plots of winding numbers versus the driving frequency is useful to analyse the complicated parameter dependence of mode-locked oscillations. For our analysis we use the generalized winding number introduced by Parlitz and Lauterborn (1987). The winding number is defined as follows. Let γ be an orbit described by the solution (x, y, z) of a system of the form

$$x' = g_1(x, y, z), \tag{3a}$$

$$y' = g_2(x, y, z), \tag{3b}$$

$$z' = \omega. \tag{3c}$$

The evolution of an infinitesimally small perturbation $(x_1(t), y_1(t), z_1(t))$ is governed by the variational equation (4) of (3).

$$\begin{pmatrix} x_1' \\ y_1' \\ z_1' \end{pmatrix} = \begin{pmatrix} \partial g_1/\partial x & \partial g_1/\partial y & \partial g_1/\partial z \\ \partial g_2/\partial x & \partial g_2/\partial y & \partial g_2/\partial z \\ 0 & 0 & 0 \end{pmatrix} \begin{pmatrix} x_1 \\ y_1 \\ z_1 \end{pmatrix}. \tag{4}$$

Since the third component of (4) has a trivial solution, $z_1 = \text{constant}$, equation (4) can be reduced to a two-dimensional system of differential equations. In terms of polar coordinates $(x_1, y_1) = (r\cos\alpha,\ r\sin\alpha)$, the variational equations of system (2) are given by

$$r' = (r/\tau_1)\cos\alpha[-\cos\alpha - AG_1(\alpha)G_2(\alpha)] + (r/\tau_2)\sin\alpha[-\sin\alpha - BG_1(\alpha)G_2(\alpha)], \tag{5a}$$

$$\alpha' = (1/\tau_2)\cos\alpha[-\sin\alpha - BG_1(\alpha)G_2(\alpha)] + (1/\tau_1)\sin\alpha[\cos\alpha + AG_1(\alpha)G_2(\alpha)], \tag{5b}$$

where

$$G_1(\alpha) = \frac{FI_{in}(1 + f\sin z)[\sin(P + x + y)/2)]}{2[1 + F\sin^2((P + x + y)/2)]^2}, \tag{5c}$$

$$G_2(\alpha) = \sin\alpha + \cos\alpha. \tag{5d}$$

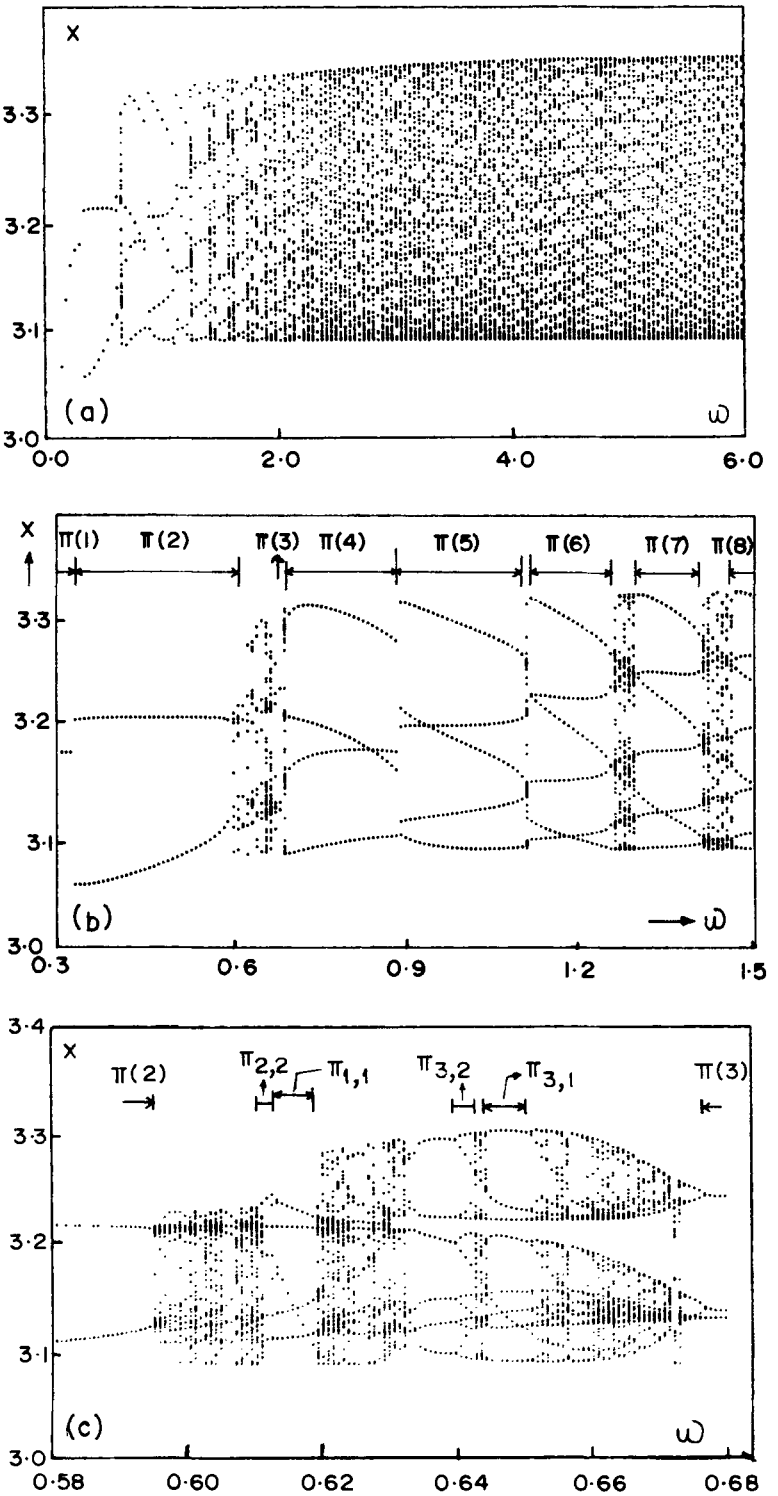

Figure 5. Bifurcation diagrams of the system (2) for $f = 0{\cdot}2$ in the Poincaré cross section onto the coordinate x versus the excitation frequency ω. (**a**) $0 < \omega < 6$, (**b**) $0{\cdot}3 < \omega < 1{\cdot}5$ and (**c**) $0{\cdot}58 < \omega < 0{\cdot}68$.

Then the mean angular velocity or the torsion frequency $\Omega(\gamma)$ of the orbit γ is given by

$$\Omega(\gamma) = \lim_{t\to\infty}(1/t)\left|\int_0^t \alpha\,dt'\right|$$

$$= \lim_{t\to\infty}(1/t)[\alpha(t) - \alpha(0)]. \tag{6}$$

The winding number $W(\gamma)$ is now defined as

$$W(\gamma) = \Omega(\gamma)/\omega. \tag{7}$$

We have computed the winding numbers corresponding to the attractors in the bifurcation diagrams 5b and 5c which are reported in figures 6a and 6b respectively. For certain intervals of ω the winding number assumes a constant rational value, that is, the system exhibits frequency-locking phenomenon. Between flat steps chaotic behavior is observed similar to the circle map (Jensen *et al* 1983) case. In the circle map the staircase was found to be monotonically increasing function of the driving strength. However, in system (2) the observed staircases are not monotonically increasing function of ω. As the angular frequency is increased the winding number increases for a while and then falls down to a lower value and then increases and so on. Figure 7a shows the 1/period (P) versus the frequency ω corresponding to the bifurcation diagram (5a) with $\Delta\omega = 6/150$. To elucidate the self-similarity in the mode-locked structure the period diagrams in the interval $\omega\in(0{\cdot}3\text{–}1{\cdot}5)$ and $\omega\in(0{\cdot}6\text{–}0{\cdot}66)$ are given in figures 7b and 7c respectively. Figure 7 clearly support Cantor-set like structure.

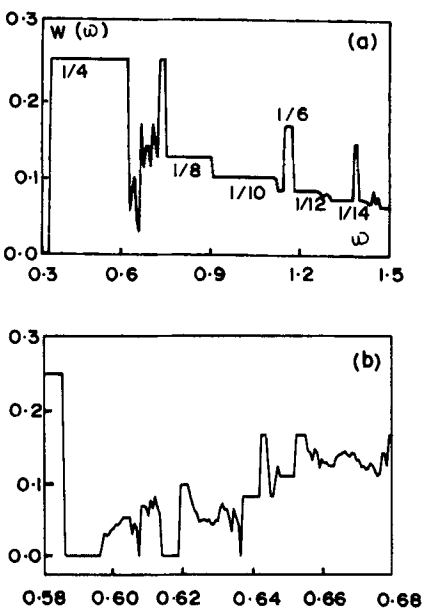

Figure 6. Winding number diagrams with $f = 0{\cdot}2$ corresponding to (**a**) figure 5b and (**b**) figure 5c.

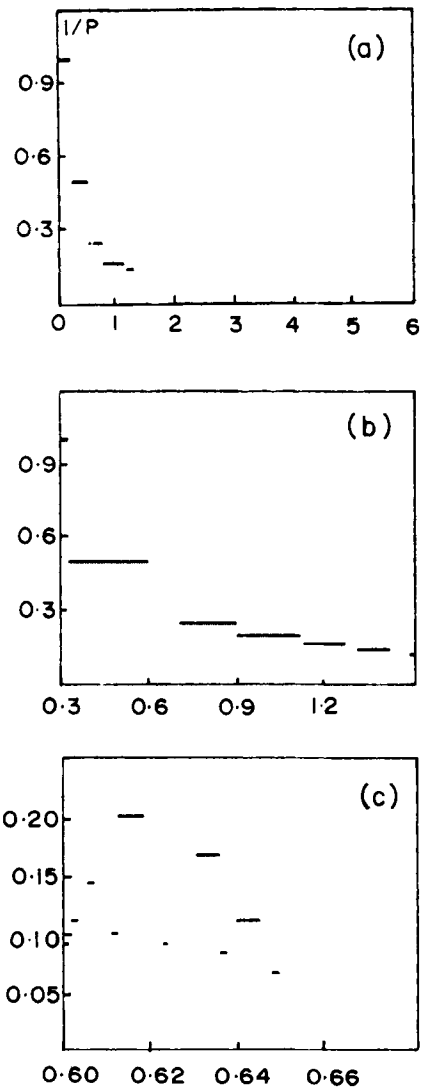

Figure 7. Period diagram with $f = 0{\cdot}2$ showing the inverse $1/P$ of the period P of the oscillation versus the excitation frequency ω for (**a**) $0 < \omega < 6$, (**b**) $0{\cdot}3 < \omega < 1{\cdot}5$ and (**c**) $0{\cdot}58 < \omega < 0{\cdot}68$.

3.4 *Period doubling bifurcations*

Period doubling bifurcation of mixed mode orbits leading to chaotic motion is also found for a range of ω values. For example, successive period doublings of (basic) period-9 attractor ($\pi_{3,1}(2, 3)$) occurs when the parameter ω is increased from 0·6544. To visualize the period doubling phenomenon, in figure 8, the values of x collected at every 9 periods of the external force are plotted against ω. Figure 8 clearly exhibits the period doubling cascade to chaos as ω is changed. At $\omega = 0{\cdot}65524$ a bifurcation occurs and a period-$9T \times 2^1$ limit cycle develops. This orbit becomes unstable at $\omega = 0{\cdot}656336$ and gives birth to a period-$9T \times 2^2$ limit cycle. Period-$9T \times 2^3$ orbit is

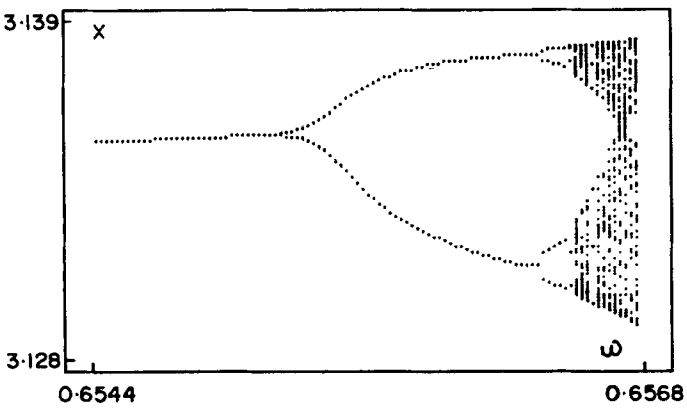

Figure 8. Bifurcation diagram illustrating the period doubling route to chaos.

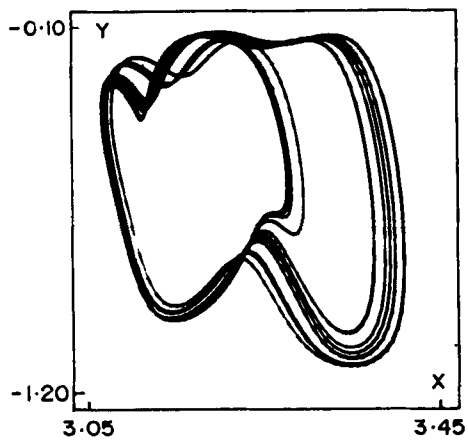

Figure 9. Chaotic orbit developed through the period doubling sequence.

observed at $\omega = 0{\cdot}656477$. Figure 9 shows the phase portrait of the chaotic orbit for $\omega = 0{\cdot}6566$.

3.5 *Quasiperiodic route to chaos*

So far, we have demonstrated the occurrence of two routes to chaos in the system (2). We have also found the quasiperiodicity-chaos transition. Figures 10a and 10c show the phase portrait and Poincaré map of typical quasiperiodic attractor for $\omega = 0{\cdot}2673$ and $f = 0{\cdot}068$. The phase portrait of the attractor is a two-torus and its Poincaré map is a closed orbit. As the parameter ω is increased transition to chaos is observed. The phase portrait and the Poincaré map of the chaotic orbit for $\omega = 0{\cdot}2774$ are given in figures 10b and 10d respectively. The points in the Poincaré map is nonuniform for the chaotic state. Here the development from the quasiperiodic motion to the chaotic motion is a process of two-torus breaking and the chaotic motion occurs for small interval of ω.

Further, in system (2) coexistence of two different attractors has also been observed for wide range of parametric choices. Figure 11a shows the chaotic orbit for $\omega = 0{\cdot}63$

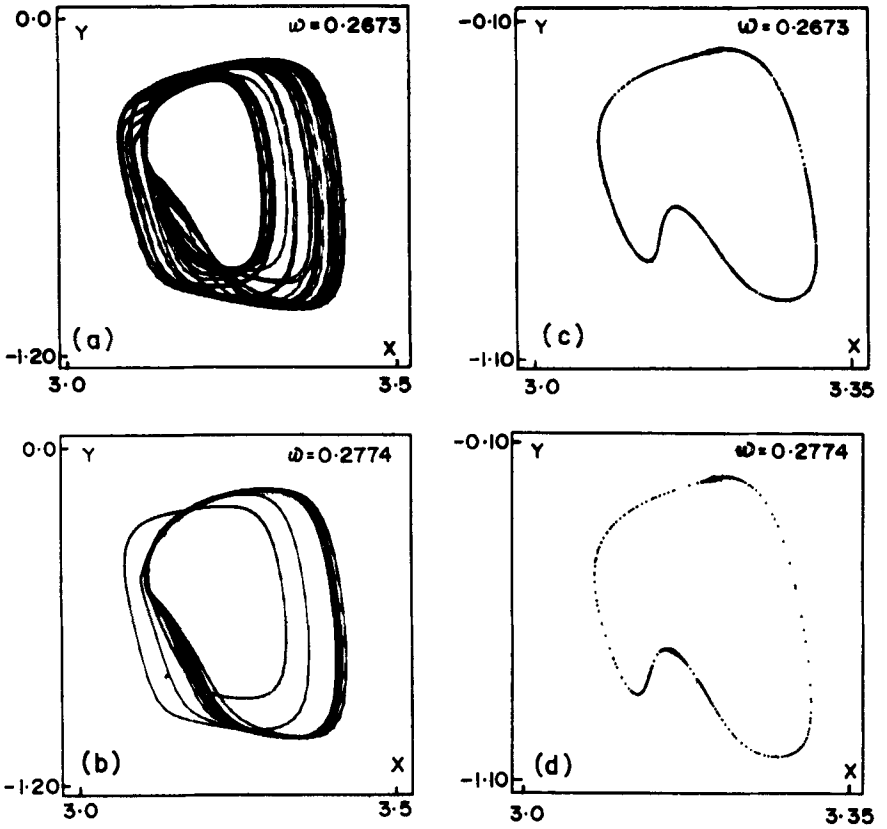

Figure 10. Phase portrait (**a**) and the Poincaré map (**c**) of the quasiperiodic attractor for $\omega = 0{\cdot}2673$ and $f = 0{\cdot}068$. Phase portrait (**b**) and the Poincaré map (**d**) of the chaotic attractor for $\omega = 0{\cdot}2774$ and $f = 0{\cdot}068$ developed through quasiperiodic route.

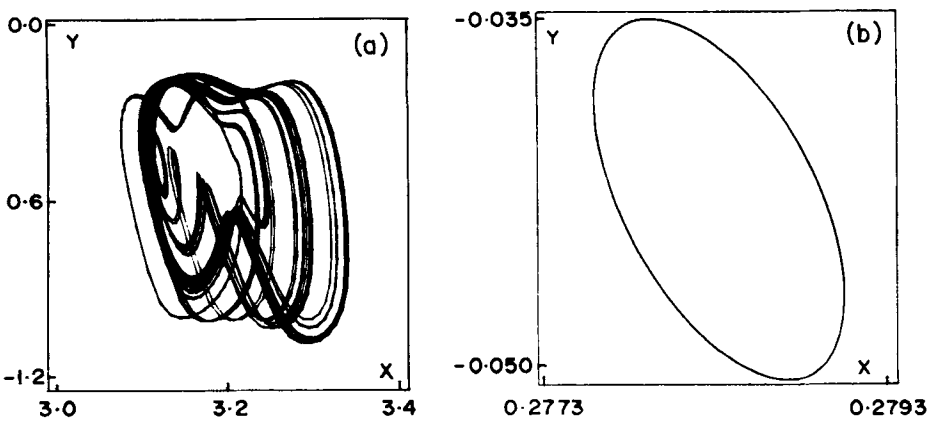

Figure 11. Two coexisting attractors for $\omega = 0{\cdot}63$ and $f = 0{\cdot}2$ (**a**) chaotic orbits and (**b**) limit cycle orbit.

with $f = 0{\cdot}2$. In addition to the chaotic orbit shown in figure 11a we have found the existence of a limit cycle attractor which is shown in figure 11b. The initial conditions used are $x(0) = 1$, $y(0) = 0{\cdot}01$. This limit cycle is found to occur for a wide range of parametric values. One can study the stability of coexisting attractors as a function of initial conditions by generating the basin boundary map.

4. Summary and conclusion

We have shown the occurrence of mode-locking phenomenon, period doubling cascades, intermittent chaos, quasiperiodic oscillations, coexistence of multiple attractors in the FPI system. The oscillator behavior in this system is essentially due to the two competing mechanisms, namely, laser-induced reorientation and laser heating of the nematic liquid crystal. In the mode-locked regime the generalized winding number has been used to describe the dynamical behavior of the system (2). The 1/period vs ω plot shows the devil's staircase scenario with Cantor-like structure. The results presented in this paper may also be amenable to experimental observations. The study of switching the actual response of the system to a desired output has a lot of practical applications in the FPI system. We are currently investigating this problem.

Acknowledgements

The author would like to acknowledge Indira Gandhi Centre for Atomic Research, Kalpakkam for providing the visiting scientist fellowship. He thanks the referee for his suggestions which improved the presentation of the paper. Part of the present work was done while the author was at the Centre for Nonlinear Dynamics, Bharathidasan University.

References

Cheung M M, Durbin S D and Shen Y R 1983 *Opt. Lett.* **8** 39
Csillag L, Janossy I, Kitaeva V F, Kroo N, Sobolev N N and Zolotko A S 1981 *Mol. Cryst. Liq. Cryst.* **78** 173
Dangoisse D, Glorieux P and Hennequin D 1990 *Phys. Rev.* **A42** 1551
Durbin S D, Arakelian S M and Shen Y R 1981a *Phys. Rev. Lett.* **47** 1411
Durbin S D, Arakelian S M and Shen Y R 1981b *Opt. Lett.* **6** 411
Durbin S D, Arakelian S M and Shen Y R 1982 *Opt. Lett.* **7** 145
Herman R M and Serinko R J 1979 *Phys. Rev.* **A19** 1757
Jensen M H, Bak P and Bohr T 1983 *Phys. Rev. Lett.* **50** 1637
Khoo I C and Zhuang S L 1982 *IEEE J. Quant. Electron* **QE-18** 246
Parlitz U and Lauterborn W 1987 *Phys. Rev.* **A36** 1428
Sasa S I 1990 *Prog. Theor. Phys.* **83** 824
Wang P, Dai J and Zhang H 1990 *Phys. Rev.* **A41** 3250
Yasin S *et al* 1991 *Intermittency and phase locking of the Bonhoeffer-van der Pol model*, Preprint
Zuniga I 1990 *Phys. Rev.* **A41** 2050